J|A|C|S
ARTICLES
Published on Web 08/10/2006

Multistep Solution-Mediated Formation of $AuCuSn_2$: Mechanistic Insights for the Guided Design of Intermetallic Solid-State Materials and Complex Multimetal Nanocrystals

Brian M. Leonard and Raymond E. Schaak*

Contribution from the Department of Chemistry, Texas A&M University, College Station, Texas 77842-3012

Received April 10, 2006; E-mail: schaak@mail.chem.tamu.edu

Abstract: Understanding how solids form is a challenging task, and few strategies allow for the elucidation of reaction pathways that are useful for designing new solids. Here, we describe an unusual multistep reaction pathway that leads to the formation of $AuCuSn_2$, a new ternary intermetallic compound that was discovered as nanocrystals using a low-temperature solution route. The formation of $AuCuSn_2$ using a modified polyol process occurs through a multistep pathway that was elucidated by taking aliquots throughout the course of the reaction and studying the products using a variety of techniques. The reaction proceeds through four distinct steps: (a) formation of Au nanoparticles at or near room temperature, mediated by a galvanic reaction between Au^{3+} and Sn^{2+} (forming Au^0 and Sn^{4+}, precipitated as SnO_2 that forms a shell around the nanoparticles), (b) formation of NiAs-type AuSn nanoparticles, along with Cu and Sn, upon addition of $NaBH_4$, (c) aggregation and thermal interdiffusion to form $AuCu_xSn_y$ alloy nanoparticles, and (d) nucleation of intermetallic $AuCuSn_2$, which has an ordered NiAs-derived structure. The proposed mechanism was tested by starting the reaction with the AuSn intermediate. AuSn nanoparticles were synthesized separately and reacted with Cu and Sn nanoparticles, and ordered $AuCuSn_2$ formed as expected. Elucidation of this reaction pathway has important implications for guiding the design of new intermetallic solids, as well as for controlling the synthesis of complex multimetal nanocrystals.

Introduction

The ability to understand how solids form is critically important for rationally designing new materials, yet the elucidation of reaction pathways remains one of the most widely recognized challenges in solid-state chemistry. Solid−solid diffusion is generally the rate limiting step in solid-state reactions, and as a result, high temperatures and long heating times are usually needed to drive the reactions to completion. Consequently, it is difficult to piece together the interactions among the reactants, including the formation of important intermediates that may be crucial for successfully forming a desired product. Furthermore, high-temperature reactions often preclude the formation of metastable and low-temperature phases that are not accessible under such conditions. The high-temperature reactions that are required for traditional solid-state syntheses, although important for generating many useful materials, have clear limitations in terms of understanding reaction pathways and stabilizing low-temperature and metastable structures.

A few general strategies exist for understanding and controlling reaction pathways in solid-state systems, and these typically involve alternative low-temperature techniques. For example, Johnson and co-workers have used elementally modulated reactants as a platform for understanding and controlling reaction pathways in thin films[1] and also for generating new solids that are inaccessible using traditional methods.[2] Topochemical strategies that modify the structures of framework solids in a stepwise and predictable manner can also be used to generate new solids via consideration of reaction pathways.[3] Understanding how low-temperature and metastable phases form could provide solid-state chemists with mechanistic guidelines for rationally designing new solids, in analogy to the retrosynthetic strategies routinely used by organic chemists.

The development of low-temperature solution routes to solid-state materials,[4−7] including strategies that yield colloidal and

(1) (a) Williams, J. R.; Johnson, M.; Johnson, D. C. *J. Am. Chem. Soc.* **2001**, *123*, 1645−1649. (b) Oyelaran, O.; Novet, T.; Johnson, C. D.; Johnson, D. C. *J. Am. Chem. Soc.* **1996**, *118*, 2422−2426. (c)Williams, J. R.; Johnson, M.; Johnson, D. C. *J. Am. Chem. Soc.* **2003**, *125*, 3489−3592. (d) Noh, M.; Johnson, C. D.; Hornbostel, M. D.; Thiel, J.; Johnson, D. C. *Chem. Mater.* **1996**, *8*, 1625−1635. (e) Schneidmiller, R.; Bentley, A.; Hornbostel, M. D.; Johnson, D. C. *J. Am. Chem. Soc.* **1999**, *121*, 3142−3149.

(2) (a) Sellinschegg, H.; Stuckmeyer, S. L.; Hornbostel, M. D.; Johnson, D. C. *Chem. Mater.* **1998**, *10*, 1096−1101. (b) Hornbostel, M. D.; Hyer, E. J.; Thiel, J.; Johnson, D. C. *J. Am. Chem. Soc.* **1997**, *119*, 2665−2668. (c) Schneidmiller, R.; Hornbostel, M. D.; Johnson, D. C. *Inorg. Chem.* **1997**, *36*, 5894−5899. (d) Hornbostel, M. D.; Hyer, E. J.; Edvalson, J. H.; Johnson, D. C. *Inorg. Chem.* **1997**, *36*, 4270−4274.

(3) (a) Stein, A.; Keller, S. W.; Mallouk, T. E. *Science* **1993**, *259*, 1558−1564. (b) Gopalakrishnan, J. *Chem. Mater.* **1995**, *7*, 1265−1275. (c) Schaak, R. E.; Mallouk, T. E. *Chem. Mater.* **2002**, *14*, 1455−1471.

(4) (a) Livage, J.; Henry, M.; Sanchez, C. *Prog. Solid State Chem.* **1988**, *18*, 259. (b) Schwartz, R. W. *Chem. Mater.* **1997**, *9*, 2325−2340. (c) Cheetham, A. K.; Mellot, C. F. *Chem. Mater.* **1997**, *9*, 2269−2279. (d) Vioux, A. *Chem. Mater.* **1997**, *9*, 2292−2299.

(5) (a) Feng, S.; Xu, R. *Acc. Chem. Res.* **2001**, *94*, 239. (b) Sheets, W. C.; Mugnier, E.; Barnabe, A.; Marks, T. J.; Poeppelmeier, K. R. *Chem. Mater.* **2006**, *18*, 7−20.

(6) Cushing, B. L.; Kolesnichenko, V. L.; O'Connor, C. J. *Chem. Rev.* **2004**, *104*, 3893−3946.

nanocrystalline solids, provides intriguing opportunities for studying solid-state formation mechanisms and accessing new structures. Along those lines, we[8−12] and others[13−15] have recently begun to explore the formation of nanocrystalline alloys and intermetallic compounds using low-temperature strategies that differ significantly from traditional high-temperature metallurgical techniques. Building on extensive work by many groups on the synthesis of metal nanoparticles using the polyol process,[6,15−18] we have been able to access a growing library of binary[11,12] and ternary[10] intermetallic compounds using modifications of this approach. The polyol process provides a low-temperature medium for precipitating reduced multimetal compounds as nanoparticles and, like most successful strategies for low-temperature solid-state synthesis, avoids solid−solid diffusion as the rate-limiting step. As anticipated from the low-temperature nature of the technique, the polyol process can also be used to generate metal and multimetal nanocrystals with new structures, including ϵ-Co[19] and Au*M*Sn$_2$ (*M* = Cu, Ni).[10]

$AuCuSn_2$ is a new ordered ternary intermetallic compound that was discovered during our initial attempts to synthesize ternary metal nanocrystals using the polyol process.[10] The Au−Cu−Sn system has been studied in detail under bulk-scale equilibrium conditions because of its importance in solder applications,[20] and interestingly, the ordered polymorph of $AuCuSn_2$ has not been observed at low temperatures (150−400 °C).[10] However, we discovered that $AuCuSn_2$ forms readily in solution below 200 °C using an unusual multistep process;[10] more common one-step polyol reactions do not yield the new intermetallic phase (Supporting Information, Figure S1). Importantly, we have been able to probe the formation mechanism by taking aliquots from the solution at various stages of the reaction and studying the crystalline and noncrystalline products, as well as the species that remain in solution. The result, presented here, is a detailed understanding of an unusual multistep reaction pathway that yields nanocrystals of a new intermetallic compound. In addition to elucidating a solid-state reaction pathway and providing a new way of thinking about the synthesis of intermetallic compounds, this work also has important implications for controlling the synthesis of complex nanocrystals.

Experimental Section

Chemicals. All chemicals were purchased from Alfa Aesar and were used as received without further processing or purification: $HAuCl_4 \cdot 3H_2O$ (99.99%), $Cu(C_2H_3O_2)_2 \cdot 2H_2O$ (98.0−102.0%), $SnCl_2$ (anhydrous, 99+% min), poly(vinyl pyrrolidone) (PVP, MW = 40 000), $NaBH_4$ (98%), and tetraethylene glycol (TEG, 99+%).

Synthesis of $AuCuSn_2$. $AuCuSn_2$ was synthesized using a modified polyol process similar to our previous report.[10] Briefly, PVP (175.0 mg), $Cu(C_2H_3O_2)_2 \cdot 2H_2O$ (21.8 mg, 0.1089 mmol), $SnCl_2$ (70.2 mg, 0.3703 mmol, 4-fold excess), and $HAuCl_4 \cdot 3H_2O$ (35.0 mg, 0.0887 mmol) were dissolved sequentially in 20 mL of TEG with sonication. This solution was stirred vigorously under bubbling Ar for a few min. The solution was then heated to 70 °C, and a freshly prepared solution of $NaBH_4$ (35 mg in 2−3 mL TEG) was added dropwise to the solution while stirring. After the metals were reduced (within 5 min), the solution was further heated to 120−200 °C. Aliquots were extracted during the reaction in order to characterize the species present at each step. Powders were collected by centrifugation and washed several times with ethanol. Acetonitrile was also used occasionally as a cosolvent to aid in precipitating all of the nanocrystalline powder from solution.

Characterization. Powder X-ray diffraction (XRD) data were collected on a Bruker GADDS three-circle X-ray diffractometer using Cu Kα radiation. Transmission electron microscopy (TEM) images, selected area electron diffraction (SAED) patterns, and energy-dispersive X-ray analysis (EDS) were collected using a JEOL JEM-2010 TEM. Elemental mapping images were acquired using a semi-STEM (STEM = scanning transmission electron microscopy) attachment. Samples were prepared by sonicating the isolated nanocrystalline powders in ethanol and dropping a small volume onto a carbon-coated nickel grid or by dropping the reaction solution directly onto the grid. Optical spectroscopy measurements were taken on a Jasco V-530 UV−visible spectrometer. Solid-state composition analysis was carried out on a four spectrometer Cameca SX50 electron microprobe.

Results and Discussion

Reaction Pathway for the Formation of $AuCuSn_2$. Figure 1 shows a schematic of the proposed multistep reaction pathway that was derived from the detailed studies that follow. Initially, the metal salt precursors and polymer stabilizer are dissolved in a high-boiling glycol solvent. Next, the polyol solvent is heated to 70 °C. This facilitates reduction of the Au^{3+} to Au^0 nanoparticles and concomitant oxidation of some of the Sn^{2+} to Sn^{4+}, which precipitates as SnO_2 nanocrystals that ultimately anneal to form a shell around the Au-containing nanoparticles. Next, $NaBH_4$ is added, which is a strong reducing agent that immediately reduces the remaining Sn^{2+} to Sn^0 and converts the Cu^{2+} to Cu^0. In this step, the Au nanoparticles appear to quickly react with the Sn to form nanocrystals of intermetallic AuSn. With further heating, the Cu^0 nanoparticles begin to aggregate and interdiffuse into the intermetallic AuSn nanocrystals, along with the remaining Sn. $AuCuSn_2$ nanocrystals form once the reaction is allowed to proceed to completion, either by controlling reaction temperature or time.

Step 1: Formation of Au Nanoparticles. After dissolving the metal salts and polymer stabilizer in TEG, the solution has a pale-yellow color (Figure 2a). Upon heating to 70 °C, the solution containing Au^{3+}, Cu^{2+}, Sn^{2+}, and PVP develops an

(7) (a) Murray, C. B.; Kagan, C. R.; Bawendi, M. G. *Annu. Rev. Mater. Sci.* **2000**, *30*, 545−610. (b) Murray, C. B.; Sun, S.; Gaschler, W.; Doyle, H.; Betley, T. A.; Kagan, C. R. *IBM J. Res. Dev.* **2001**, *45*, 47−56.
(8) Sra, A. K.; Schaak, R. E. *J. Am. Chem. Soc.* **2004**, *126*, 6667−6672.
(9) Schaak, R. E.; Sra, A. K.; Leonard, B. M.; Cable, R. E.; Bauer, J. C.; Han, Y.-F.; Means, J.; Teizer, W.; Vasquez, Y.; Funck, E. S. *J. Am. Chem. Soc.* **2005**, *127*, 3506−3515.
(10) Leonard, B. M.; Bhuvanesh, N. S. P.; Schaak, R. E. *J. Am. Chem. Soc.* **2005**, *127*, 7326−7327.
(11) Sra, A. K.; Ewers, T. D.; Schaak, R. E. *Chem. Mater.* **2005**, *17*, 758−766.
(12) Cable, R. E.; Schaak, R. E. *Chem. Mater.* **2005**, *17*, 6835−6841.
(13) (a) Vondrova, M.; Klimczuk, T.; Miller, V. L.; Kirby, B. W.; Yao, N.; Cava, R. J.; Bocarsly, A. B. *Chem. Mater.* **2005**, *17*, 6216−6218. (b) Vondrova, M.; Majsztrik, P. W.; Gould, S.; Bocarsly, A. B. *Chem. Mater.* **2005**, *17*, 4755−4757.
(14) Cokoja, M.; Parala, H.; Schroter, M. K.; Birkner, A.; van den Berg, M. W. E.; Grunert, W.; Fischer, R. A. *Chem. Mater.* **2006**, *18*, 1634−1642.
(15) Roychowdhury, C.; Matsumoto, F.; Mutolo, P. F.; Abruna, H. D.; DiSalvo, F. J. *Chem. Mater.* **2005**, *17*, 5871−5876.
(16) (a) Fievet, F.; Lagier, J. P.; Blin, B.; Beaudoin, B.; Figlarz, M. *Solid State Ionics* **1989**, *32/33*, 198−205. (b) Ducamp-Sanguesa, C.; Herrera-Urbina, R.; Figlarz, M. *Solid State Ionics* **1993**, *63−65*, 25−30.
(17) (a) Toshima, N.; Kushihashi, K.; Yonezawa, T.; Hirai, H. *Chem. Lett.* **1989**, *10*, 1769−1772. (b) Toshima, N.; Harada, M.; Yamazaki, Y.; Asakura, K. *J. Phys. Chem.* **1992**, *96*, 9927−9933. (c) Toshima, N.; Yonezawa, T. *New J. Chem.* **1998**, 1179−1201.
(18) (a) Sun, Y.; Wiley: B.; Li, Z.-Y.; Xia, Y. *J. Am. Chem. Soc.* **2004**, *126*, 9399−9406. (b) Wiley: B.; Herricks, T.; Sun, Y.; Xia, Y. *Nano Lett.* **2004**, *4*, 1733−1739. (c) Wiley: B.; Sun, Y.; Mayers, B.; Xia, Y. *Chem.−Eur. J.* **2005**, *11*, 454−463. (d) Kim, F.; Connor, S.; Song, H.; Kuykendall, T.; Yang, P. *Angew. Chem., Int. Ed.* **2004**, *43*, 3673−3677.
(19) Dinega, D. P.; Bawendi, M. G. *Angew. Chem., Int. Ed.* **1999**, *38*, 1788−1791.
(20) (a) Roeder, J. F.; Notis, M. R.; Goldstein, J. I. *Defect Diffus. Forum* **1988**, *59*, 271−278. (b) Karlsen, O. B.; Kjekshus, A.; Rost, E. *Acta Chem. Scand.* **1990**, *44*, 197−198. (c) Peplinski, B.; Zakel, E. *Mater. Sci. Forum* **1994**, *166−169*, 443−448. (d) Karlsen, O. B.; Kjekshus, A.; Rost, E. *Acta Chem. Scand.* **1992**, *46*, 147−156.

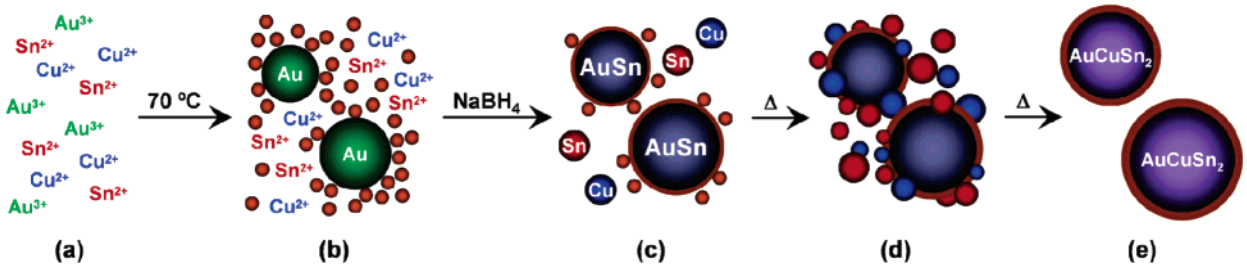

Figure 1. Schematic of the proposed multistep reaction pathway for the formation of $AuCuSn_2$ nanocrystals: (a) metal salt reagents (with PVP in TEG), (b) formation of Au and SnO_2 nanoparticles (the small orange spheres represent SnO_2, resulting from a galvanic reaction between Au^{3+} and Sn^{2+} that forms Au^0 and Sn^{4+}, which precipitates as SnO_2), (c) formation of NiAs-type AuSn nanoparticles, along with Sn and Cu, (d) aggregation and thermal interdiffusion to form $AuCu_xSn_y$ alloy nanoparticles, and (e) nucleation of intermetallic $AuCuSn_2$. In (c), (d), and (e), the orange-colored shell on the AuSn, $AuCu_xSn_y$, and $AuCuSn_2$ nanoparticles, respectively, represents the SnO_2 coating that forms from annealing the SnO_2 nanoparticles in solution, and it persists throughout the entire reaction.

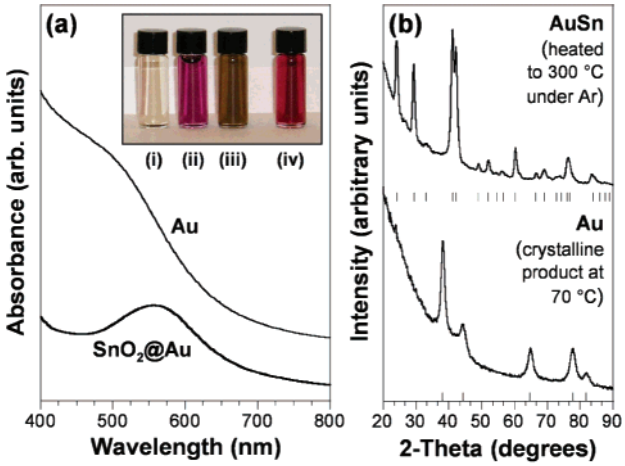

Figure 2. (a) Visible absorption spectra showing that the SPR band for the red-colored solution of Au nanoparticles is centered around 520 nm and the SPR band for the purple-colored Au−Cu−Sn solution heated to 70 °C is centered at 555 nm. The SPR peak for the Au−Cu−Sn solution is red-shifted relative to that of Au due to the presence of SnO_2 nanoparticles in solution, which interact with the surface of the Au nanoparticles. The inset shows a photograph of (i) the metal salts (Au^{3+}, Cu^{2+}, Sn^{2+}) dissolved in solution, (ii) the purple-colored solution after heating to 70 °C, (iii) the heated solution reduced by $NaBH_4$, and (iv) a control (red-colored) solution of Au nanoparticles formed by $NaBH_4$ reduction. (b) Powder XRD patterns for the solid product precipitated from the Au−Cu−Sn reaction solution heated to 70 °C (bottom) and the same powder annealed at 300 °C in a tube furnace under Ar (top), showing the formation of intermetallic AuSn from the Au−Sn nanocomposite. Tick marks below each pattern represent the allowed Bragg reflections for Au (bottom) and NiAs-type AuSn (top).

intense-purple color (Figure 2a), which suggests the formation of metal nanoparticles that have a visible surface plasmon resonance (SPR) peak. This is confirmed by UV−visible spectroscopy (Figure 2a). Interestingly, when a solution containing only Au^{3+} and PVP is heated to 70 °C in TEG, no visible reaction occurs. However, when reduced with $NaBH_4$, the solution turns wine red and exhibits a SPR peak centered around 520 nm (Figure 2a), which is consistent with the well-known SPR peak of spherical Au nanoparticles.[21] The optical data suggests subtle but important differences between the Au−Cu−Sn sample (purple) and the pure Au sample (red), and these differences are probed and understood by utilizing several complementary techniques that are described below.

The powder XRD pattern for the solid product isolated from the purple Au−Cu−Sn solution by solvent-induced precipitation and centrifugation, yielding a clear colorless solvent, shows only

(21) (a) Mulvaney, P. *Langmuir* **1996**, *12*, 788−800. (b) Link, S.; Wang, Z. L.; El-Sayed, M. A. *J. Phys. Chem. B* **1999**, *103*, 3529−3533.

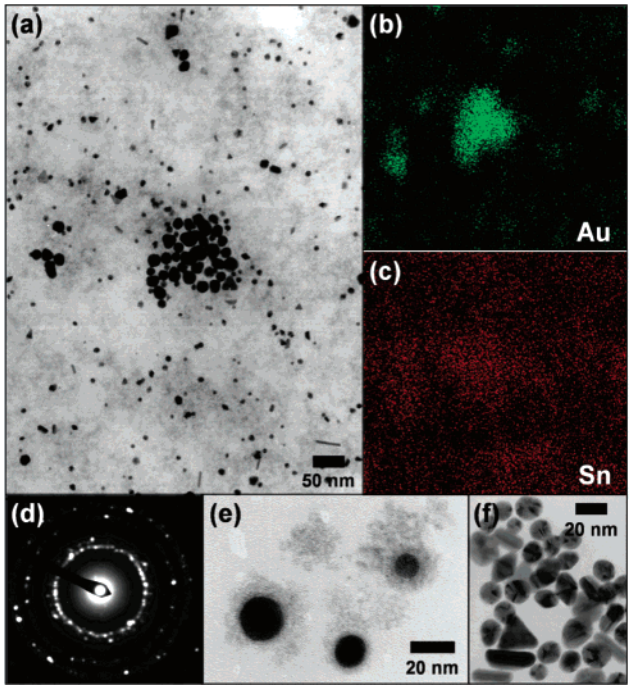

Figure 3. (a) TEM micrograph for the Au−Cu−Sn reaction solution heated to 70 °C, showing the presence of Au (larger, high contrast) and SnO_2 (small, medium contrast) nanoparticles. (b) and (c) Semi-STEM elemental mapping data for the TEM micrograph in panel (a), showing that Au is present in the high contrast areas (b) and Sn is present in the areas of medium contrast (c). (The lowest contrast regions represent the background.) The SAED pattern in (d) shows an fcc pattern matching that of Au. The TEM micrograph in (e) shows a close-up of Au nanoparticles surrounded by smaller SnO_2 particles (facilitated by solution-phase annealing), and the micrograph in (f) shows Au nanoparticles that were isolated without a SnO_2 coating by using low-speed centrifugation.

nanocrystalline Au (Figure 2b). However, electron microprobe analysis of the solid product shows the presence of both Au and Sn in a 1.00:0.96 ratio. The Cu content of this sample is below the detection limit of the instrument, which indicates that Au and Sn are incorporated into the product but Cu is not.

Careful analysis by TEM reveals several additional details. The TEM micrograph in Figure 3, prepared by dropping the purple-colored Au−Cu−Sn solution directly onto a TEM grid, shows high-contrast nanoparticles that range in size from 5 to 30 nm. The SAED pattern (Figure 3d) shows an fcc pattern that is consistent with that expected for Au and also agrees with the XRD data shown in Figure 2b. However, a significant amount of diffuse contrast surrounding the Au nanoparticles implies that other smaller nanoparticles are present in the solid

product. Qualitative EDS analysis shows that both Au and Sn are present, consistent with the electron microprobe data. Elemental mapping of the TEM micrograph in Figure 3a shows that Au is only present in the high-contrast regions (Figure 3b), whereas Sn is also present in the regions of diffuse contrast that surround the Au particles (Figure 3c). This indicates that the Au nanoparticles are loosely surrounded by smaller Sn-containing nanoparticles.

Interestingly, if the TEG solution containing Au^{3+}, Sn^{2+}, and Cu^{2+} is *not* heated, it also turns purple over a short period of time (Supporting Information, Figure S2). The same color change occurs when no Cu is present. Considering the standard reduction potentials of Au^{3+}/Au [$E° = 1.498$ eV vs. standard hydrogen electrode (SHE)] and Sn^{4+}/Sn^{2+} ($E° = 0.151$ eV vs. SHE), we hypothesize that a spontaneous galvanic reaction occurs, in which Au^{3+} is reduced to Au^0 as Sn^{2+} is oxidized to Sn^{4+}, precipitated as SnO_2 (because the reaction is not performed under rigorously air-free conditions). Furthermore, a higher-magnification TEM image confirms the presence of 2−3 nm SnO_2 particles (Supporting Information, Figure S3). Apparently, Au and SnO_2 nanoparticles are mixed in solution, and they form a nanoscale composite when the solution is dropped onto a TEM grid (Figure 3a). Importantly, when this solid composite product is annealed under Ar at 300 °C, the XRD pattern matches that of intermetallic AuSn (Figure 2b), which is further evidence that the Au and Sn are mixed in a 1:1 ratio in the solid product and in solution. We speculate that the SnO_2 remains unreactive and does not participate in the subsequent steps (as will be shown below). However, its presence (the result of a galvanic reaction between Sn^{2+} and Au^{3+}) is the result of a critical reaction that helps to reduce the Au^{3+} to Au^0 at a much lower temperature than would normally occur in a standard polyol reaction. Furthermore, the fact that Au and SnO_2 nanoparticles can be generated at room temperature implies that the polyol solvent is not the reducing agent. Rather, this further supports the hypothesis that a galvanic reaction is responsible for the formation of Au nanoparticle seeds.

Returning to the UV−visible spectroscopy data shown in Figure 2a, the red-shift in the SPR peak for the Au−Cu−Sn sample relative to that of the Au sample, making the Au−Cu−Sn solution purple instead of red, can be explained by the nanostructure of the sample. The Au nanoparticles are surrounded by smaller SnO_2 nanoparticles in a pseudo core−shell composite arrangement. Mulvaney and co-workers have studied this in detail, observing a red-shift of the SPR band as Au nanoparticles are coated by a SnO_2 shell; the shift in the SPR peak is related to the thickness of the SnO_2 coating.[22] In their system, the SnO_2@Au nanoparticle solution is purple instead of red,[22] which matches what we observe. Indeed, after solution-phase annealing of our SnO_2/Au nanoparticle mixture, core−shell SnO_2@Au aggregates are clearly observed (Figure 3e). However, if a low centrifugation speed is used prior to annealing, the constituent Au nanoparticles can be removed without the SnO_2 coating (Figure 3f), implying that the core−shell structure is dynamic in solution rather than fully passivating the surface. Furthermore, at the intermediate centrifugation speeds typically used, the SnO_2 that is attached to the Au nanoparticles can be isolated along with the Au, but some remains in solution because of its small size. Thus, the amount

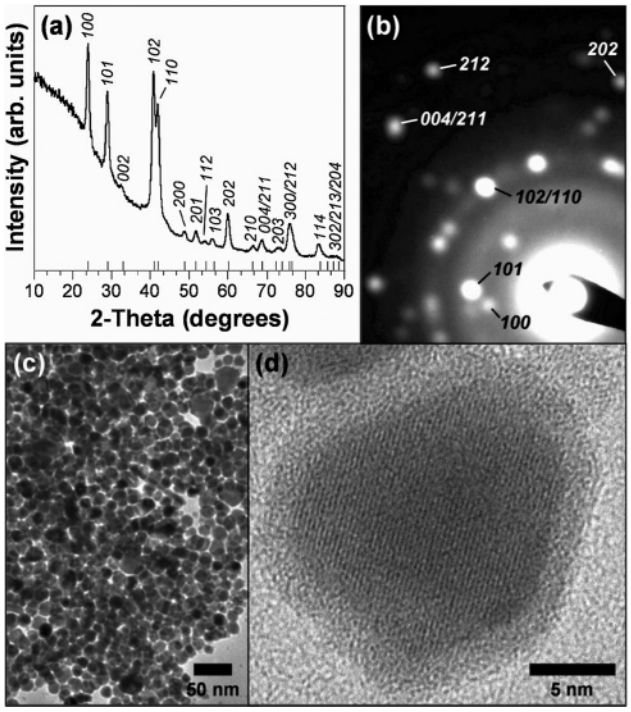

Figure 4. (a) Powder XRD and (b) SAED pattern of the solid product isolated after heating to 70 °C and reducing by $NaBH_4$. Tick marks below the XRD pattern in (a) represent the allowed Bragg reflections for NiAs-type AuSn. The TEM micrograph in (c) shows the morphology of the AuSn nanocrystals, and (d) shows a representative single AuSn nanocrystal, which has a single-crystal core and a 1−2 nm SnO_2 shell.

of SnO_2 present in the centrifuged sample is less than the total amount of SnO_2 present in the system. Although a complete galvanic reaction between Sn^{2+} and Au^{3+} would require 1.5 mol of Sn^{2+} for every mole of Au^{3+}, the centrifuged sample does not isolate all of the SnO_2. Consequently, the electron microprobe data that shows a 1.00:0.96 ratio of Au/Sn for the centrifuged sample is reasonable, based on this analysis.

Taken together, the UV−vis, XRD, TEM, and electron microprobe data are consistent with the initial formation of Au nanoparticles via a galvanic reaction between Au^{3+} and Sn^{2+}, which ultimately forms SnO_2 nanoparticles. Also, the data imply that Cu is does not participate in the initial reaction.

Step 2: Formation of AuSn Nanoparticles. When the reaction solution turns purple (e.g., reaches 70 °C or is allowed to react at room temperature), a solution of $NaBH_4$ is added dropwise and the Au−Cu−Sn solution immediately turns dark brown (Figure 2a), which implies reduction of other species in solution. In control experiments, Cu^{2+} and Sn^{2+} can both be reduced to Cu^0 and Sn^0 nanoparticles, respectively, under these conditions (70 °C in TEG upon addition of $NaBH_4$). The powder XRD pattern of the precipitate from this reaction, isolated by centrifugation, shows exclusively the formation of intermetallic NiAs-type AuSn (Figure 4a). Indeed, electron microprobe analysis of the centrifuged product finds a Au/Sn/Cu ratio of 1.00:1.32:0.15, which is consistent with the presence of nanocrystalline AuSn, some of the SnO_2 generated in the first step (specifically, the approximate fraction of the total SnO_2 that is incorporated into a core−shell structure as described below), and very little Cu or extra Sn. Indeed, after centrifuging all of the solid products, the supernatant retains a brown color, which is consistent with the presence of small nanoparticles of Cu and Sn that remain in solution. No well-defined SPR band is

(22) Oldfield, G.; Ung, T.; Mulvaney, P. *Adv. Mater.* **2000**, *12*, 1519−1522.

observed by UV−visible spectroscopy, but this is not unexpected, because Cu nanoparticles smaller than 4 nm do not show a distinct SPR peak[23] and the SPR band for Sn nanoparticles is primarily in the UV.[24] Taken together, these data imply that the Cu remains in solution and does not appreciably incorporate into the AuSn product and that reduced Sn nanoparticles are also present in solution.

TEM micrographs of the AuSn nanoparticles are shown in Figure 4c. The nanoparticles, which are mostly ∼20 nm but range in size from 5 to 40 nm, are generally single-crystal AuSn and have a clearly defined core−shell structure (Figure 4d) that results from solution-phase annealing of the SnO_2 nanoparticles onto the AuSn surface. (Our previous work with the $FeSn_2$ system showed analogous SnO_2 shells on most Sn-based nanoparticles synthesized using a similar polyol-based approach.[12]) SAED (Figure 4b) shows the hexagonal NiAs structure expected for the AuSn core. Furthermore, XPS analysis (not shown) shows the presence of primarily oxidized Sn on the surface with very little signal from Au or Cu, consistent with a thin coating of SnO_2 on the majority of the particles. Based on these data, we propose that the core is intermetallic AuSn and the shell is amorphous SnO_2.

This step in the reaction pathway is surprising but important, and it is significant for several reasons. First, intermetallic AuSn forms very quickly at 70 °C, which is a lower temperature than is required to crystallize most other related intermetallics we have synthesized using similar methods.[10−12] Second, the fact that Au forms first and then converts to AuSn when $NaBH_4$ is added implies that the Au nanoparticles are highly reactive with the reduced Sn, and that the presence of Au seeds may catalyze the nucleation of intermetallic AuSn. Finally, AuSn crystallizes in the NiAs structure, which is the structure from which ordered $AuCuSn_2$ is derived. The NiAs-type AuSn intermediate may provide a structural template for the formation of ordered $AuCuSn_2$ at low temperatures. Taken together, the data presented above are consistent with the formation of a core−shell SnO_2@AuSn intermediate with small Cu and Sn nanoparticles present in solution.

Step 3: Interdiffusion to Form an $AuCu_xSn_y$ Alloy. At this point in the reaction (at 70 °C and after $NaBH_4$ is added), the solution appears to contain a mixture of SnO_2@AuSn, Cu, and Sn nanoparticles. As a control experiment, we confirmed that SnO_2 nanoparticles dispersed in TEG with $NaBH_4$ do *not* convert to Sn^0 at temperatures up to 300 °C (Supporting Information, Figure S5). Thus, we conclude that the SnO_2 nanoparticles do not react or incorporate into the product, so they remain inert in solution. The remainder of the Sn necessary to convert AuSn into $AuCuSn_2$ comes from the Sn^{2+} that is reduced to Sn^0 by $NaBH_4$. This conclusion is also consistent with the large 4-fold excess of Sn^{2+} that is used to form $AuCuSn_2$. Per mole of $AuCuSn_2$, 1.5 mol of Sn are required to reduce all of the Au^{3+} to Au^0, concomitantly oxidizing Sn^{2+} to Sn^{4+}. An additional mole of Sn is required to reduce and react with the Au nanoparticles to form AuSn. Another mole of Sn (along with one mole of Cu) is required to form $AuCuSn_2$ from AuSn. Thus, 3.5 mol of Sn are required based on our proposed reaction pathway, and 4.0 mol are routinely used. Experimentally, we found that $AuCuSn_2$ will not form with less than 3.6 mol of Sn, which agrees well with the proposed reaction pathway and the amount of Sn it requires.

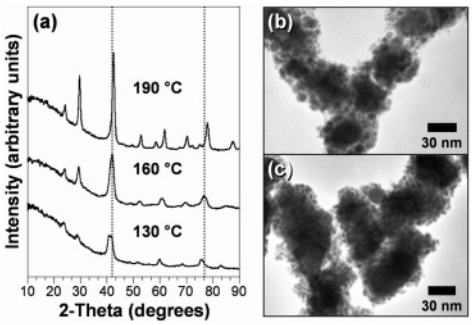

Figure 5. (a) Powder XRD patterns for the products isolated as a function of increasing temperature. The progressive shift of the lattice constants highlights the diffusion of Cu and Sn into the AuSn nanoparticles. TEM micrographs of the aliquots taken at (b) 85 °C and (c) 120 °C show larger AuSn particles that are surrounded by smaller particles, which are likely Cu, Sn, and Cu_xSn_y.

As heating continues in the presence of reduced Sn and Cu, the particles continue to interact and react, which is similar to the reaction of Au with Sn to form AuSn. The result is the evolving formation of $AuCu_xSn_y$ alloy nanoparticles, which have variable compositions that change with temperature (Figure 5a) and time (Supporting Information, Figure S6) as the reaction progresses. Continual incorporation of Sn and Cu into the alloy nanoparticles is likely facilitated by the enhanced diffusivity and reactivity inherent in nanoparticle systems.[25] The thermal interdiffusion of Cu and Sn into AuSn can be monitored using powder XRD of the solid products that are isolated from aliquots taken at different temperatures (Figure 5a). At 130 °C, the lattice constants are $a = 4.29$ Å and $c = 5.34$ Å, and the unit cell becomes progressively smaller as the temperature is increased to 160 °C ($a = 4.24$ Å, $c = 5.25$ Å) and 190 °C ($a = 4.23$ Å, $c = 5.23$ Å). This is consistent with the diffusion of Cu into the structure, because Cu is smaller than both Au and Sn. (The lattice constants of the $AuCu_xSn_y$ alloy at 190 °C agree with those of ordered $AuCuSn_2$, implying that diffusion is nearly complete by this point and that the composition is close to $AuCuSn_2$.)

TEM micrographs of the Au−Cu−Sn particles in the 85−120 °C range show larger 30−40 nm particles surrounded by smaller particles that are typically 5−10 nm in diameter (Figure 5b,c). EDS mapping confirms that Au, Cu, and Sn are present in the clusters of particles (Figure 6). Thus, based on the available data, we hypothesize that the smaller particles on the periphery of the larger ones are Cu, Sn, or Cu−Sn alloys, and that they continually interdiffuse and incorporate into the larger particles as a function of time and temperature, consistent with the available data.

Step 4: Formation of Intermetallic $AuCuSn_2$. As the solution continues heating, diffusion continues until the stoichiometry reaches $AuCuSn_2$, and the ordered ternary structure forms. The XRD pattern in Figure 7a shows the characteristic superlattice peaks of the ordered $AuCuSn_2$ structure, which appear above 190 °C. Ordered $AuCuSn_2$ can also be accessed at temperatures as low as 120 °C, if the solution is heated at this temperature for at least 1 h (Figure S6). Importantly, the

(23) Lisiecki, I.; Pileni, M. P. *J. Phys. Chem.* **1995**, *99*, 5077−5082.
(24) Henglein, A.; Giersig, M. *J. Phys. Chem.* **1994**, *98*, 6931−6935.
(25) (a) Yin, Y.; Rioux, R. M.; Erdonmez, C. K.; Hughes, S.; Somorjai, G. A.; Alivisatos, A. P. *Science* **2004**, *304*, 711−714. (b) Son, D. H.; Hughes, S. M.; Yin, Y.; Alivisatos, A. P. *Science* **2004**, *306*, 1009−1012.

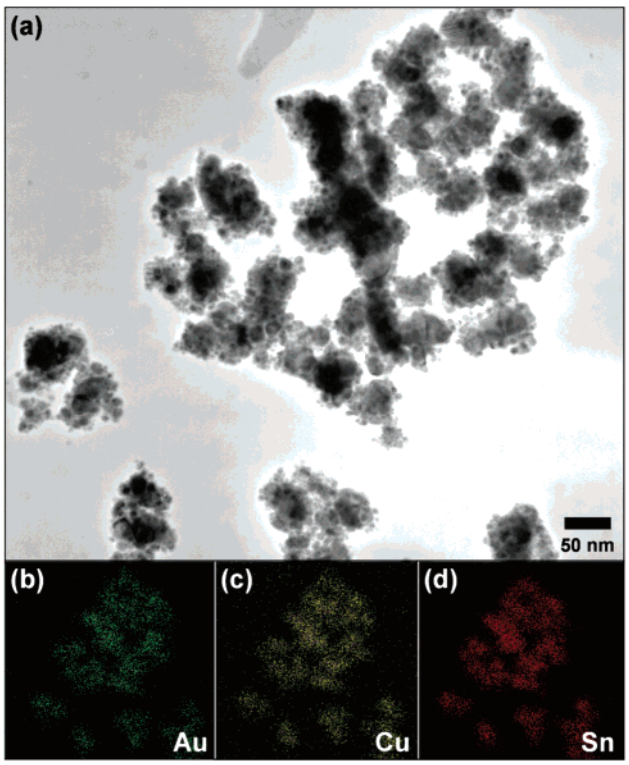

Figure 6. (a) TEM micrograph of the product isolated at 85 °C, and semi-STEM elemental mapping data that shows the presence of (b) Au, (c) Cu, and (d) Sn in each of the aggregates.

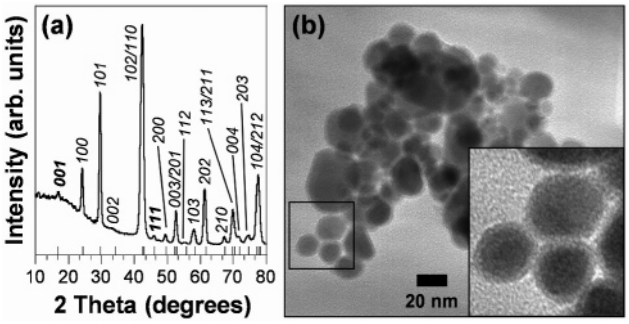

Figure 7. (a) Powder XRD pattern of intermetallic $AuCuSn_2$ isolated at 190 °C. Tick marks below the pattern show the positions of the allowed Bragg reflections, and the reflections in boldface type highlight the most prominent superlattice peaks of $AuCuSn_2$ (see ref 10 for details). (b) TEM micrograph of the $AuCuSn_2$ powder isolated at 190 °C. The inset reveals that the core−shell structure is still present on the final product.

$AuCuSn_2$ nanocrystals have a core−shell structure (Figure 7b), which implies that the SnO_2 coating does indeed persist throughout the reaction, as shown schematically in Figure 1.

Testing and Confirming the Reaction Pathway. The results above, characterizing each of the steps involved in the formation of ordered $AuCuSn_2$ nanocrystals, provide compelling evidence that $AuCuSn_2$ forms by (a) nucleating Au nanoparticles from Au^{3+} via a galvanic reaction with Sn^{2+}, (b) reacting the Au nanoparticles with Sn to form intermetallic AuSn nanocrystals, (c) incorporating the additional Sn and Cu into the AuSn nanocrystals via solution-mediated interdiffusion, and (d) nucleation of the ordered $AuCuSn_2$ structure when the 1:1:2 stoichiometry has been reached. If this is indeed the correct reaction pathway, it should be possible to begin the reaction at any of the intermediate steps and drive the reaction to completion, e.g., formation of ordered $AuCuSn_2$. Accordingly, Figure 8 shows

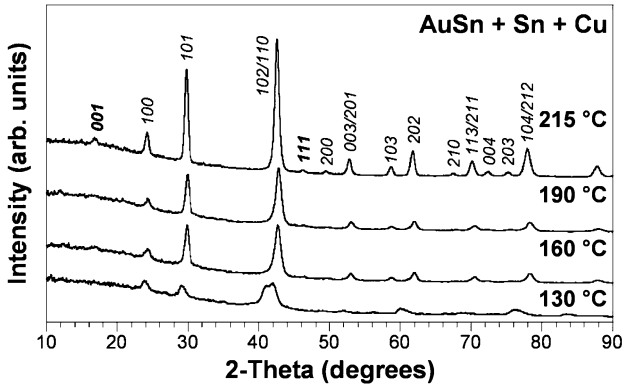

Figure 8. Powder XRD patterns for the products isolated from the reaction of a physical mixture of AuSn (along with excess Sn) with a solution of Cu nanoparticles that were formed ex situ. The patterns show temperature-dependent changes in lattice constants that are similar to those seen in the original reaction that began with all of the metal salts in solution. Intermetallic $AuCuSn_2$ is formed by 215 °C, and the reflections in boldface type highlight the most prominent superlattice peaks of $AuCuSn_2$.

that ordered $AuCuSn_2$ can be formed by first synthesizing AuSn nanocrystals (in the presence of excess Sn as discussed earlier), then thermally reacting them in solution with Cu nanoparticles that are formed ex situ.

In this alternate scenario, $HAuCl_4$ and $SnCl_2$ are dissolved in TEG with PVP as a surface stabilizing agent. This solution is heated to 70 °C to form a purple solution similar to that formed when all three metal salts were present. As expected from the reaction pathway, the XRD pattern for the solid product isolated from this solution by centrifugation matches that of nanocrystalline Au. Furthermore, TEM micrographs show a mixture of Au and SnO_2 nanoparticles that look similar to the product isolated from the original three-component system (Supporting Information, Figure S4). This unambiguously establishes that Cu is not implicated in the first step of the reaction. When $NaBH_4$ is added, AuSn nanoparticles are formed, again without any Cu present in the solution. In a separate vial, a solution of $Cu(C_2H_3O_2)_2$ and PVP in TEG are reduced with $NaBH_4$, forming a brown solution of Cu nanoparticles. This solution is then added to the solution of AuSn nanoparticles (containing excess Sn) and heated to 215 °C. Both the XRD pattern (Figure 8) and the SAED pattern (Figure 9a) for the product of this reaction match that of the ordered ternary $AuCuSn_2$ structure, which forms after the Cu nanoparticles react with the AuSn nanoparticles. Furthermore, the progression of XRD patterns from 130 to 215 °C in Figure 8 shows the same evidence for interdiffusion (e.g., progressive evolution of the lattice constants) as the original sample. Finally, the $AuCuSn_2$ nanoparticles made by this method also contain a SnO_2 shell, consistent with the proposed reaction pathway (Figure 9). Taken together, these results prove that $AuCuSn_2$ can be made directly from a physical mixture of AuSn and Cu nanoparticles (in the presence of excess Sn), and provide compelling evidence that the reaction pathway described in Figure 1 is reliable.

Applicability to Other Systems. Although our proposed multistep reaction pathway is clearly applicable to the formation of $AuCuSn_2$, it is important to consider its generality for other systems. As a first step toward this goal, we studied the formation of $AuNiSn_2$. Although $AuNiSn_2$ is structurally similar to $AuCuSn_2$,[10] the synthesis, stability, and reactivity of metal

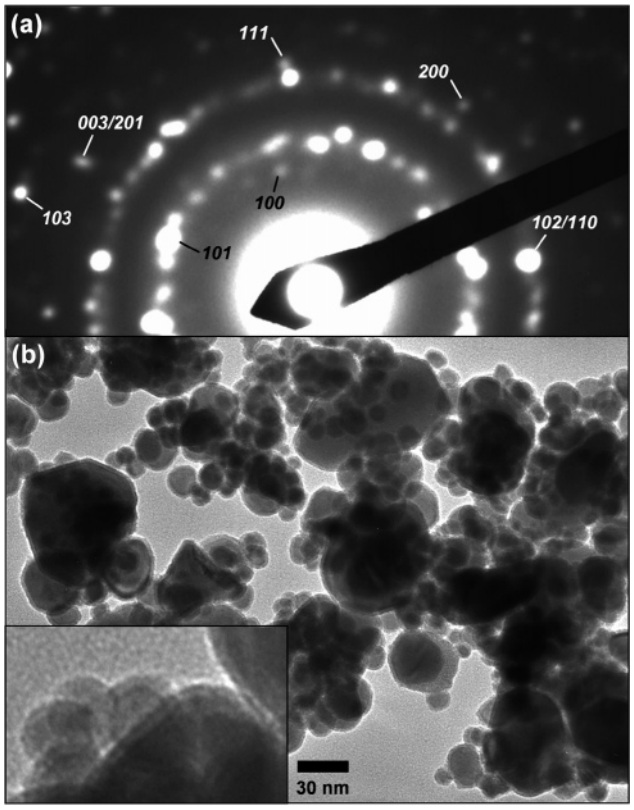

Figure 9. (a) SAED pattern and (b) TEM micrograph of the intermetallic $AuCuSn_2$ powder isolated at 215 °C from the reaction of AuSn with Sn and Cu.

nanoparticles can often be different for each element,[26] so it is worthwhile to compare the Ni and Cu systems. Like $AuCuSn_2$, ordered $AuNiSn_2$ appears to only form in solution from a careful multistep reaction sequence that is analogous to the one shown in Figure 1. After dissolving appropriate amounts of $HAuCl_4 \cdot 3H_2O$, $Ni(C_2H_3O_2)_2 \cdot xH_2O$, and $SnCl_2$ in TEG, the color of the solution changes from yellow to red-brown as the temperature is increased to 85 °C. Powder XRD data for the solid product isolated from this reaction shows the presence of nanocrystalline Au (Figure 10), consistent with the first step of the pathway required to form $AuCuSn_2$. After adding $NaBH_4$, the color changes to black, and the XRD and SAED patterns are consistent with those expected for AuSn (Supporting Information, Figure S7), although the particles are significantly smaller than those observed for the $AuCuSn_2$ system. As the temperature is further increased, the XRD peaks sharpen and shift systematically with temperature (Figure 10), suggesting diffusion to form disordered $AuNi_xSn_y$ nanoparticles. Finally, by 210 °C, the characteristic superlattice peaks are clearly evident (Figure 10), indicating the formation of ordered $AuNiSn_2$.

The isolation of intermediates that are similar to those obtained for the $AuCuSn_2$ system imply that the reaction pathway of $AuNiSn_2$ is also similar, which gives an indication of its generality to other new, yet related, systems. We are currently in the process of testing this reaction pathway with other systems, and preliminary evidence suggests that it will

(26) (a) Ely, T. O.; Amiens, C.; Chaudret, B.; Snoeck, E.; Verelst, M.; Respaud, M.; Broto, J.-M. *Chem.* Mater. **1999**, *11*, 526−529. (b) Hyeon, T. *Chem. Commun.* **2003**, 927−934. (c) Cushing, B. L.; Kolesnichenko, V. L.; O'Connor, C. J. *Chem. Rev.* **2004**, *104*, 3893−3946. (d) Green, M. *Chem. Commun.* **2005**, 3002−3011.

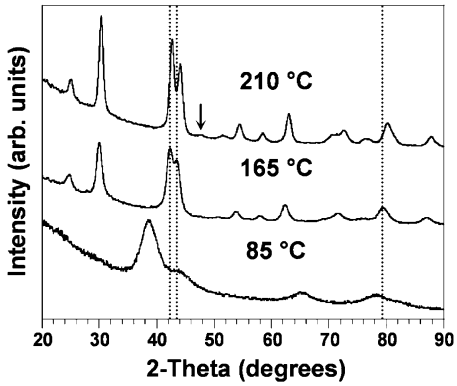

Figure 10. Powder XRD patterns for the products isolated as a function of increasing temperature for the Au−Ni−Sn system. (Bottom) Au nanoparticles isolated at 85 °C, (Middle) $AuNi_xSn_y$ isolated at 165 °C, and (Top) ordered $AuNiSn_2$ isolated at 210 °C (the arrow highlights one of the key superlattice peaks). The dashed lines highlight the peak shifting that occurs with heating, indicative of interdiffusion.

indeed result in the formation of new nanocrystalline alloys and intermetallic compounds, including in systems that are structurally and compositionally distinct from the Au*M*Sn_2 phases. Thus, we reasonably anticipate that this reaction pathway will be applicable to other systems. However, even if this particular reaction pathway turns out not to be overly general, it still provides important new insights into how nanoparticles combine in solution, in a controllable manner, to form derivative compounds with more complex structures and compositions. As such, it provides guidelines for systematically modifying the structures and compositions, and thus the properties, of nanocrystalline intermetallic compounds.

Conclusions

In this paper, we identified and tested a plausible multistep reaction pathway that results in the formation of a new ternary intermetallic compound, $AuCuSn_2$, as nanocrystalline particles. Our experiments identified four key reaction steps: (a) formation of a mixture of Au and SnO_2 nanoparticles mediated by a spontaneous galvanic reaction between Au^{3+} and Sn^{2+}, (b) formation of SnO_2-coated AuSn nanoparticles, along with small particles of Cu and Sn, upon $NaBH_4$ reduction, (c) temperature-controlled interdiffusion to form $AuCu_xSn_y$ nanoparticles, and (d) nucleation of the ordered ternary structure of $AuCuSn_2$, which retains a coating of SnO_2. Consistent with this mechanism, $AuCuSn_2$ can also be formed by starting with the AuSn intermediate and reacting it with Cu and Sn.

Elucidation of the reaction pathway that is required to form $AuCuSn_2$ has several important implications. First, it provides a rare look at the steps involved in the formation of a new solid-state compound, and these mechanistic insights could provide valuable tools for the guided design of other new intermetallic solids. In particular, the formation of NiAs-type AuSn as an intermediate is important and may help to template the low-temperature formation of $AuCuSn_2$, which is an ordered variant of the NiAs structure. Second, it demonstrates a novel strategy for studying mechanistic details of solid-state phase formation at the nanometer scale by combining data from multiple complementary techniques, including microscopy, spectroscopy, and diffraction. Although the approach and tools are quite different from those necessary to elucidate molecular reaction mechanisms, the result is analogous—a systematic piece-by-

piece look at the interactions of small building blocks to form a larger structure—and has similar implications in terms of applying the mechanism to other systems. Third, the reaction pathway provides a strategy for fine-tuning the composition and structure of multimetal nanocrystals in a more systematic and controllable manner than is routinely achievable using one-pot reactions. Indeed, the ability to react metal and intermetallic nanoparticles in solution to form derivative phases could open up new doors for the guided design of compositionally and structurally complex nanocrystals, and preliminary evidence with other systems suggests that it can. Fourth, there are several strategies for controlling the shape and size of single-metal nanocrystals,[18,27] but analogous achievements for multimetal systems remain rare. Because the formation of $AuCuSn_2$ begins with the nucleation of Au nanoparticles, it may be possible to control nanocrystal size and shape of this ternary intermetallic compound (or other complex phases) by starting with pre-made Au nanocrystals that have the appropriate morphological characteristics.

Finally, this study effectively merges what were thought to be two distinct strategies for synthesizing alloys and intermetallic compounds using low-temperature "metallurgy in a beaker" techniques. In one approach, metal nanoparticles are mixed in known ratios in solution to form nanocomposites, which precipitate and are heated as dry powders to form alloys and intermetallics of predetermined compositions.[8,9] In this case, the rapid low-temperature reactivity is attributed to the nanoscale diffusion distances afforded by the self-assembled precursors that form in solution, which mimic the mixing achieved by the high temperature melting step usually required in traditional metallurgical synthesis. In the other approach, alloy and intermetallic nanocrystals are formed using modifications of the polyol process, which traditionally uses the polyol solvent as the reducing agent, but in some cases can also utilize stronger reducing agents (e.g., $NaBH_4$).[10−12] The multistep reaction pathway presented here provides compelling evidence that a nanocomposite forms in solution and transforms into alloy and intermetallic nanocrystals via solution-mediated reactions. Essentially, the two approaches are the same—both involve the formation and interdiffusion of nanoscale composites of two or more distinct phases. The approaches appear to differ only in the method used to interdiffuse the components, e.g., dry powder processing vs solution annealing. A similar mechanism may end up being implicated in the formation of other multimetal nanocrystals formed by reacting metal salt precursors in high-boiling solvents, and may possibly turn out to be general for the formation of other multimetal nanocrystals using low-temperature solution routes.

Acknowledgment. This work was supported by the National Science Foundation (DMR-0545201), the Robert A. Welch Foundation (Grant No. A-1583), and start-up funds from Texas A&M University. Acknowledgment is also made to the Donors of the American Chemical Society Petroleum Research Fund for partial support of this research. Electron microscopy was performed at the Microscopy and Imaging Center at Texas A&M University. The electron microprobe was partially funded by the DOE.

Supporting Information Available: Powder XRD patterns for the attempted formation of $AuCuSn_2$ using various one-pot polyol reactions; photograph of Au−Cu−Sn solution after reacting for 15 min at room temperature; enlarged TEM micrographs of the Au and SnO_2 nanoparticles present in the purple-colored solution; TEM micrograph of the Au and SnO_2 nanoparticles present in the solution containing only Au and Sn (with no Cu); powder XRD patterns showing the effect of heating SnO_2 nanoparticles in TEG with $NaBH_4$, as well as the time-dependent formation of $AuCuSn_2$ at 120 °C; XRD, TEM, and SAED data for the AuSn intermediate isolated during the formation of $AuNiSn_2$. This material is available free of charge via the Internet at http://pubs.acs.org.

JA062475H

(27) (a) Chen, S.; Wang, Z. L.; Ballato, J.; Foulger, S. H.; Carroll, D. L. *J. Am. Chem. Soc.* **2003**, *125*, 16186−16187. (b) Sau, T. K.; Murphy, C. J. *J. Am. Chem. Soc.* **2004**, *126*, 8648−8649. (c) Hao, E.; Bailey, R. C.; Schatz, G. C.; Hupp, J. T.; Li, S. *Nano Lett.* **2004**, *4*, 327−330.